



CHORUS

This is the accepted manuscript made available via CHORUS. The article has been published as:

Stable-unstable transition for a Bose-Hubbard chain coupled to an environment

Chu Guo, Ines de Vega, Ulrich Schollwöck, and Dario Poletti

Phys. Rev. A **97**, 053610 — Published 16 May 2018

DOI: [10.1103/PhysRevA.97.053610](https://doi.org/10.1103/PhysRevA.97.053610)

Stable-unstable transition for a Bose-Hubbard chain coupled to an environment

Chu Guo,¹ Ines de Vega,² Ulrich Schollwöck,² and Dario Poletti¹

¹*EPD Pillar, Singapore University of Technology and Design, 8 Somapah Road, 487372 Singapore*

²*Department of Physics and Arnold Sommerfeld Center for Theoretical Physics, Ludwig-Maximilians-University Munich, 80333 Munich, Germany*

Interactions in quantum systems may induce transitions to exotic correlated phases of matter which can be vulnerable to coupling to an environment. Here, we study the stability of a Bose-Hubbard chain coupled to a bosonic bath at zero and non-zero temperature. We show that only above a critical interaction the chain loses bosons and its properties are significantly affected. The transition is of a different nature than the superfluid-Mott insulator transition and occurs at a different critical interaction. We explain such a stable-unstable transition by the opening of a global charge gap. The comparison of accurate matrix product state simulations to approximative approaches that miss this transition reveals its many-body origin.

I. INTRODUCTION

Interactions lead to emergent collective phenomena and quantum phase transitions in soft and condensed matter systems. However, real systems are often coupled to an environment, and therefore we need to understand how this affects the system properties. The environment may destroy key properties of the isolated system e.g. due to decoherence or to particle losses. Recent experiments with ultracold atoms have started investigating these phenomena [1–5]. The interplay between system and environment can even be tailored to generate interesting non-equilibrium phases of matter [6, 7].

In this work, we focus on the robustness of a many body quantum system against the coupling to an external bath: We consider a one-dimensional Bose-Hubbard chain (BHC) which exhibits a quantum phase transition between a superfluid phase and a Mott-insulating phase driven by interaction strength and particle density [8–10]. We study the dissipative dynamics of the BHC after coupling its last site to a bosonic bath either at zero or non-zero temperature, while we also show that our results can be extended to the case in which the BHC is coupled to a bosonic bath at every site. Dissipation is often modeled by a Lindblad master equation [11, 12] which implies a number of assumptions on the system, the bath(s) and their coupling [13–15]. The Lindblad master equation assumes weak coupling to and instantaneous recovery of the environment (Markov approximation), which makes the system-environment state separable (Born approximation). If separability is lost, one has to go beyond a Lindblad master equation approach. For this reason, the Hamiltonian dynamics of the system plus bath has been studied recently in spin systems [16, 17]. In other cases, the dynamics of two connected spin or bosonic chains prepared in different states was investigated [18–21]. Quantum Monte Carlo approaches have also proven to be very insightful [22, 23].

Convenient methods to study both equilibrium and non-equilibrium properties of 1D systems are matrix product states (MPS) based algorithms which can be modified to include the dissipative effects of an envi-

ronment as described by the Lindblad formalism or the equivalent Markovian quantum jump approach [24–27]. Here we use an MPS algorithm to study an interacting bosonic system coupled to a bosonic bath at either zero or finite temperature. Our analysis is, to the best of our knowledge, the first to tackle this problem without assuming a Born-Markov approximation. To facilitate the numerics we characterize the bath thermal state by performing a thermofield transformation [28]. Moreover, we consider a unitary transformation that maps the environment into a chain structure containing only nearest-neighbor tunnelling [29–31].

We show that for a zero-temperature bath the system is stable against the dissipation only if the interaction is below a certain threshold, while the system loses bosons for a larger interaction. For non-zero temperatures the evolution changes drastically depending, again, on the strength of the interaction. In this case the system's number of bosons can increase on numerically accessible time scales for sufficiently weak interactions. These effects are purely many-body as they cannot be described by simple mean-field approaches. Moreover we show that a Redfield master equation approach, which is accurate at short times, cannot predict the stable-unstable transition. We should also stress that this instability transition produced by the system-bath coupling, is of different nature than the ground-state superfluid to Mott-insulator phase transition. In fact it is due to a different mechanism, which we explain later, and occurs at a different critical interaction strength.

The paper is structured as follows: in Sec. II we present the model, in Sec. III we discuss how we analyze it and in Sec. IV we discuss the stability of the system. In Sec. V we focus on the long time dynamics and in Sec. VI we draw our conclusions.

II. MODEL

We consider a BHC coupled to an environment of free bosonic oscillators. The Hamiltonian of the system plus

environment can be written as

$$\hat{H}_{\text{tot}} = \hat{H}_S + \hat{H}_E + \hat{H}_I, \quad (1)$$

with \hat{H}_S being the Hamiltonian of a BHC of length L , tunnelling amplitude J and onsite interaction strength U

$$\hat{H}_S = -J \sum_{j=1}^{L-1} (\hat{\alpha}_j^\dagger \hat{\alpha}_{j+1} + \text{H.c.}) + \frac{U}{2} \sum_{j=1}^L \hat{\alpha}_j^\dagger \hat{\alpha}_j (\hat{\alpha}_j^\dagger \hat{\alpha}_j - 1). \quad (2)$$

To have lighter notations, henceforth we work in units such that $J = \hbar = k_B = 1$. We are interested in the relaxation dynamics of the system starting from the ground state of average filling $\bar{n} = 1$, which we denote as $|E_{N=L}^0\rangle$, where N is the total number of bosons in the system. In 1D the transition from superfluid to Mott-insulator occurs at the critical value $U_c \approx 3.37$ [32]. The L -th site of the BHC is coupled to an environment of harmonic oscillators, whose Hamiltonian can simply be written as $\hat{H}_E = \int d\omega \omega \hat{b}_\omega^\dagger \hat{b}_\omega$. We consider a coupling between the system and the environment of the form

$$\hat{H}_I = \int d\omega \sqrt{\mathcal{J}(\omega)} \left(\hat{\alpha}_L^\dagger \hat{b}_\omega + \hat{\alpha}_L \hat{b}_\omega^\dagger \right) \quad (3)$$

where $\mathcal{J}(\omega) = g\omega^\eta$ is the spectral density and it corresponds to a sub-ohmic, ohmic, or super-ohmic bath respectively for $\eta < 1$, $\eta = 1$ or $\eta > 1$ [15, 33]. We choose a sharp cut-off of the spectral density ω_{max} such that $\mathcal{J}(\omega) = 0$ for $\omega > \omega_{\text{max}}$. The environment is prepared in a thermal state with temperature T , i.e. $\hat{\rho}_E \propto e^{-\hat{H}_E/T}$.

To apply MPS methods we need to discretize the environment. We use a linear discretization of the bath [34] into N_{max} oscillators evenly spaced by $\Delta\omega = \omega_{\text{max}}/N_{\text{max}}$, resulting in $\hat{H}_E^{\text{dis}} = \sum_{j=1}^{N_{\text{max}}} \omega_j \hat{b}_j^\dagger \hat{b}_j$, with $\omega_j = j\Delta\omega$. At the same time, \hat{H}_I becomes $\hat{H}_I^{\text{dis}} = \sum_{j=1}^{N_{\text{max}}} \sqrt{\mathcal{J}_j} (\hat{\alpha}_L^\dagger \hat{b}_j + \hat{\alpha}_L \hat{b}_j^\dagger)$, with $\mathcal{J}_j = \int_{\omega_j}^{\omega_{j+1}} d\omega \mathcal{J}(\omega) \approx \mathcal{J}(\omega_j) \Delta\omega$ and we have used $\hat{b}_j \equiv \hat{b}_{\omega_j}$. We have tested the convergence for different values of $\Delta\omega$ choosing $\Delta\omega = 0.01$ and $\omega_{\text{max}} = 6$.

III. METHOD

For a bath at temperature $T = 0$, we map the discretized bath to a long linear non-interacting bosonic chain with nearest-neighbor couplings [30, 31, 34, 35]. The full Hamiltonian of the system is therefore represented as a long chain in which the first $L = 10$ sites correspond to the BHC and the next sites (200 in our simulations) correspond to the transformed environment oscillators. The full system wave function is then evolved accordingly from the initial condition $|\psi\rangle = |E_{N=L}^0\rangle \otimes |0\rangle_c$ where $|0\rangle_c$ is the vacuum of the \hat{c}_j , the annihilation operators of free bosons on the chain representing the discretized bath [35, 36], while $|E_{N=L}^0\rangle$ is the ground state

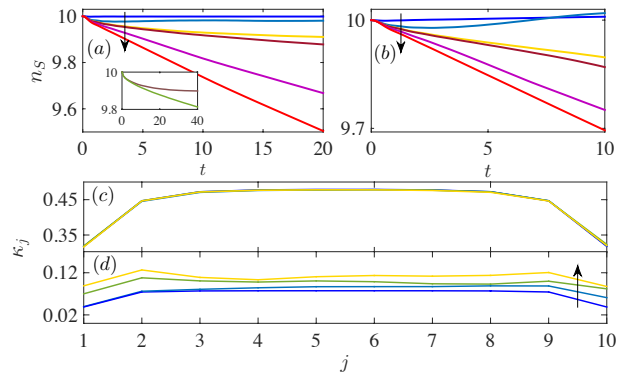


FIG. 1: (color online) (a,b) Total number of bosons in the system as a function of time t for (a) $T = 0$ and (b) $T = 0.1$. The lines in the direction of the arrow correspond to $U = 0, 2, 2.8, 2.9, 4, 10$. The inset of (a) shows a detail for $U = 2.8$ and 2.9 for longer times. (c,d) Local fluctuations κ_j as a function of site j , for $U = 2$ and $U = 10$, for different times: in the direction of the arrow $t = 0, 4, 10, 16, 20$ (in (c) the lines are on top of each other). In all panels, the other bath parameters used in both cases are $g = 0.01$ and $\eta = 0.5$. For all panels we have $N = L = 10$.

for the BHC with N atoms on L sites. We use a second-order Suzuki-Trotter split-step method with time step $dt = 0.01$, bond dimension 4000, and local basis dimension 5 in the bath; in the system it is 7 for $U = 1$, 6 for $1 < U \leq 4$, 5 for $U > 4$.

For $T > 0$, we first perform a thermofield transformation [28], in which the finite temperature environment is exactly mapped to two virtual environments at zero temperature. These two environments are then unitarily transformed to two different chains of oscillators having nearest-neighbor coupling and annihilation (creation) operators $\hat{a}_{1,j}$ and $\hat{a}_{2,j}$ ($\hat{a}_{1,j}^\dagger$ and $\hat{a}_{2,j}^\dagger$) respectively. The total state to be evolved can then be written as $|\psi\rangle = |E_{N=L}^0\rangle \otimes |0\rangle_{a_1} \otimes |0\rangle_{a_2}$, where $|0\rangle_{a_1}$, $|0\rangle_{a_2}$ are the vacuum states of all the $\hat{a}_{1,j}$ and $\hat{a}_{2,j}$ corresponding to the two thermofield environments (see [28, 35] for details). The parameters used for the simulations are the same as for $T = 0$ except that we use a non-number conserving algorithm with a bond dimension 300, and swap gates [37] to implement the 2nd order Suzuki-Trotter evolution.

IV. STABILITY OF THE SYSTEM

In order to understand the dynamics of this many body system we need to consider the *global set-up* made of the BHC, which we will refer to as the *system*, and the environment or *bath*. The system Hamiltonian, \hat{H}_S , conserves the total number of bosons while the bath couples different number sectors. Since initially $N = L$, and given the type of system-bath coupling (3), the environment will first induce transitions to states with $N = L \pm 1$ bosons. If such transitions are allowed by energy conservation of

the *global set-up*, then the system is unstable, but if there is a *global energy gap* for the *system+bath* set-up, then the system will be stable.

We analyze the stability of the ground state of the system by monitoring the number of bosons in the BHC

$$n_S(t) = \sum_{j=1}^L \langle \psi(t) | \hat{\alpha}_j^\dagger \hat{\alpha}_j | \psi(t) \rangle. \quad (4)$$

As shown in Fig.1(a,b), when the interaction strength U varies the evolution of $n_S(t)$ changes substantially.

At $T = 0$, see Fig.1(a), the environment does not have bosons to transfer to the system, so the number of bosons in the system can only change from $N = L$ to $N = L - 1$. The key is thus to study the energy difference between the ground state energy of the system $E_{N=L}^0$, and the ground state energy $E_{N=L-1}^0$ corresponding to $N = L - 1$ atoms, i.e. $\Delta E = E_{N=L}^0 - E_{N=L-1}^0$. This is the largest amount of energy that the system can lose when the first boson is removed. For large values of U , $\Delta E > 0$. The transfer of a boson from the system to the bath can occur because the system loses energy while the bath gains energy and hence the overall energy of the system plus bath can be conserved. However for low enough interaction $\Delta E < 0$. This implies that if the system loses a boson it also gains energy, while the bath would always gain energy by gaining a particle. Hence there is an energy gap for the *global set-up* which results in an almost completely frozen dynamics of the system [38].

The different response of the system to the bath is also well evidenced by the system's local fluctuations $\kappa_j = \langle (\hat{\alpha}_j^\dagger \hat{\alpha}_j)^2 \rangle - \langle \hat{\alpha}_j^\dagger \hat{\alpha}_j \rangle^2$, a quantity which can be studied with state-of-the-art experiments. For low interaction, Fig.1(c) with $U = 2$, the fluctuations change minimally (the curves for different times are superimposed), while for larger interactions, Fig.1(d) with $U = 10$, there is a sizable "fluctuation wave" starting at site $j = 10$, where the bath is connected, and propagating in the system.

The transition from stable to unstable dynamics is clearly highlighted in Fig.2(a,b) where we plotted the decay slope θ from a linear fit of n_S for $2 < t < 20$ for various values of the interaction strength U [39]. Each line corresponds to a different type of bath, sub-ohmic ($\eta = 1/2$), ohmic ($\eta = 1$) and super-ohmic ($\eta = 2$). In all scenarios there is a clear transition between non-decaying and decaying dynamics. Computing $\Delta E = 0$ for systems up to $L = 120$, we identify the transition to occur at $U_s \approx 2.82$ [40]. We shall note that such value is consistent with the change in sign of the chemical potential computed in [32]. Such transition line at $U = U_s$ is highlighted by a black-dashed line in Fig.2. With the red-dotted line instead we show U_c , the critical interaction strength for the superfluid-Mott insulator transition, which is clearly larger than the interaction strength at which the stable-unstable transition occurs. In Fig.2(c), by plotting ΔE vs U for $L = 10$, we clearly show that $\Delta E > 0$ for large U and it is negative for smaller interaction strength [41]. In Fig.2(b) we zoom into Fig.2(a)

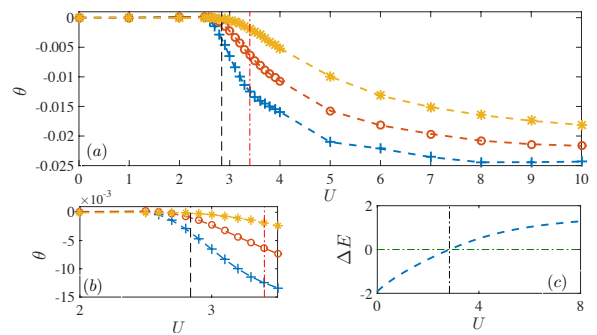


FIG. 2: (color online) (a) θ , the slope of the evolution of $n_S(t)$ as a function of U . Each line corresponds to a different spectral density: blue crosses for $\eta = 0.5$ (sub-ohmic), red circles for $\eta = 1$ (ohmic) and yellow stars for $\eta = 2$ (super-ohmic) while $g = 0.01, 0.01, \text{ and } 0.01$ respectively. The vertical black-dashed line highlights the critical value of the interaction $U = U_s$ while the red dot-dashed line shows U_c , the location of the quantum phase transition between superfluid and Mott-insulator. (b) Detail of (a) near the stable/unstable critical interaction. In panels (a,b) we have $N = L = 10$. (c) Groundstates energy difference ΔE versus U and for $L = 10$.

around the transition point. Since the coupling to the environment produces a shift in the energy levels, the transition point may be shifted. Such shift is particularly significant for the sub-ohmic bath, as it effectively produces a stronger coupling.

We stress that the difference in the critical value of the stable-unstable ($U_s \approx 2.82$) and superfluid-Mott insulator ($U_c \approx 3.37$) transitions is not due to a bath-induced renormalization of the interaction U as in [42]. There the system-bath coupling is number-conserving which results in completely different physics. For instance their system is more robust to dissipation when U is larger.

A. Non-zero temperature of the bath

The dynamics ensuing the coupling to a $T > 0$ bath presents important similarities and differences compared to a $T = 0$ bath. In Fig. 1(b) we show the number of particles in the system n_S as a function of time for different interaction strengths U . The most important difference compared to the $T = 0$ case is that the bosonic modes in the bath are not in the vacuum but they are populated. This implies that there are energy conserving processes for which boson goes from the bath to the system and hence the number of particles in the system can increase. At large U and for the time scales observed, the loss of particles, which is possible because $\Delta E > 0$, is still the dominating effect. For smaller U instead, as shown in particular in Fig. 1(b) for $U = 0, 2$, the dominant dynamics similar to the $T = 0$ case, is such that the number of bosons increases in the system while it decreases in the bath.

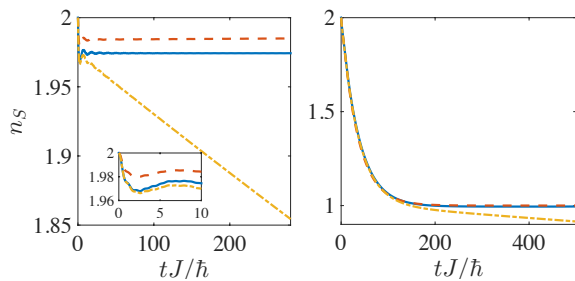


FIG. 3: (color online) Total number of bosons in the system as a function of t for (a) weak interaction $U = 1$ (the inset focuses on the short-time dynamics) and (b) strong interaction $U = 5$. The environment has temperature $T = 0$, and we have used $g = 0.01$ and $\eta = 0.5$. The blue continuous line, dashed red line, and yellow dot-dashed line correspond respectively to the MPS results, the effective model, and the Redfield equation. For all panels we have $N = L = 2$.

V. LONG TIME DYNAMICS

In order to gain a clear insight into the long time dynamics we now study a smaller system with $T = 0$ and $N = L = 2$. This allows us to reach $t = 500$. Fig.3 shows the system's particle number for (a) small and (b) large interactions. For such a small system we can also study the evolution of the reduced density matrix of the system using the Redfield master equation, which is a second order weak coupling master equation that requires the Born but not the Markov approximation. As shown in Fig.3 (see also the inset), the Redfield equation is accurate at short times but predicts the wrong steady state both for weak and strong interactions U , even though the coupling between the system and the environment is relatively weak, $g = 0.01$. The disagreement is particularly important for weak interactions for which the exact dynamics predicts a stable dynamics while the Redfield master equation predicts a decay. For larger U , for which the system can lose bosons, the Redfield equation is accurate up to much longer times, but eventually it still predicts decay [43].

In order to obtain qualitatively correct results, an approach which accounts well for the system-bath correlations that are built up is needed. For the two-site case, where only a few energy levels are relevant for the system dynamics, we can use an effective model based on the ground states corresponding to $N = 1$ and $N = 2$ bosons in the system (see [35]). The prediction of this effective model is shown with red dashed lines in Fig. 3 and indeed matches qualitatively the exact numerical results of MPS simulations. The coupling strength g , and the particular typology of the spectral density \mathcal{J} , do not have a qualitative effect on the stable-unstable transition, which only becomes sharper for weaker coupling. In Fig.4(a) we show the number of bosons for different interaction strengths. We then fit these curves with an exponential decay $n_S(t) - n_S(\infty) \propto e^{-t/\tau}$ with $n_S(\infty) = 1$ to esti-

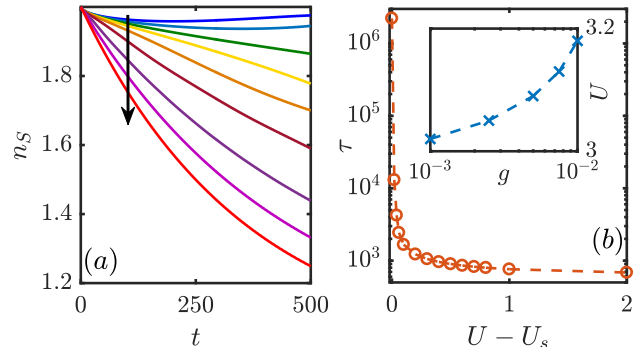


FIG. 4: (color online) (a) Total number of bosons in the system as a function of t for $T = 0$, $g = 0.001$. The lines in the direction of the arrow correspond to $U = 3, 3.02, 3.04, 3.06, 3.1, 3.2, 3.5, 4, 5$. (b) The relaxation time τ as a function of $U - U_s$ for $g = 0.001$. The inset shows the variation of the critical interaction U_s with the strength of the coupling of the system to the bath g in a lin-log plot. For all panels we have $N = L = 2$.

mate the time scale τ . In Fig.4(b) we plot this time scale versus the interaction U minus the critical interaction U_s for a small $g = 0.001$. Clearly the time scale changes dramatically as the interaction approaches U_s , especially for $g = 0.001$, indicating that a very different dynamics occurs for lower interactions. The exact value of the critical interaction U_s varies with the interaction strength g , and this dependence is shown, in a lin-log form, in the inset of Fig. 4(b).

It is important to stress that this stable-unstable transition cannot be predicted by simpler meanfield approaches. For instance, a Gutzwiller ansatz [10, 44, 45] to study a Mott-insulator coupled to a $T = 0$ bath predicts a completely frozen dynamics with no decay, which is qualitatively inaccurate [46]. Within a cluster meanfield approach for the system, the dynamics would not be completely frozen, however it would be significantly slowed down for large U , which is also qualitatively wrong.

VI. CONCLUSIONS

We have studied the stability of a Bose-Hubbard chain coupled to a thermal bosonic bath. We have shown that at $T = 0$, when varying the on-site interaction strength between the bosons in the BHC across a critical value U_s , there is a transition between stable to unstable dynamics. This transition is due to a change in sign of the difference between the ground state energies of a system with $N = L$ (corresponding to the initial state) and $N = L - 1$ bosons. The stable-unstable transition occurs at lower values of the interaction compared to the equilibrium quantum-phase transition between a superfluid and a Mott-insulator, showing that the two transitions, while both due to the on-site interaction U , are of dis-

tinct nature. We have also shown that the many body nature of these effects goes beyond both a Redfield master equation and simple meanfield approaches.

This system can be realized experimentally with atoms in two hyperfine states, one which is trapped by a lattice and one which is not and forms a reservoir as described in [47]. The great flexibility of digital micromirror devices [48] together with atom microscopes would also allow the experimental realization of the same physics. Alternatively, the bosonic bath could be excitations within a BEC while the system is formed by impurities [49]. Most importantly, since the stable-unstable transition is due to the presence of a global energy gap that can prevent the loss of a boson from the system, it can be observed also if *each* site of the system is coupled to the bath [35]. This makes the set-up much closer to possible experimental realizations.

The stable-unstable transition may also signal the presence of a non-equilibrium phase transition in the steady state. In fact the steady state will be markedly different in the two sides of the transition, as it is highlighted for instance by the different total number of bosons in the system. However our current tools do not allow us to reach the steady state for a large number of atoms and show this. Future work may consider systems with richer phase diagrams than the Bose-Hubbard chain.

Acknowledgments: D.P. acknowledges support from Ministry of Education of Singapore AcRF MOE Tier-II (project MOE2016-T2-1-065, WBS R-144-000-350-112) and fruitful discussions with B. Grémaud. D.P. was hosted by ICTP during part of this study. This work was performed in part at the Aspen Center for Physics, which is supported by NSF grant PHY-1607611. I. de V. further acknowledges support by the DFG-grant GZ: VE 993/1-1 and discussions with A. Recati.

-
- [1] G. Barontini, R. Labouvie, F. Stubenrauch, A. Vogler, V. Guarrera, and H. Ott, *Phys. Rev. Lett.* **110**, 035302 (2013).
- [2] Y.S. Patil, S. Chakram, and M. Vengalattore *Phys. Rev. Lett.* **115**, 140402 (2015).
- [3] R. Labouvie, B. Santra, S. Heun, and H. Ott, *Phys. Rev. Lett.* **116**, 235302 (2016).
- [4] H. P. Luschen, P. Bordia, S. S. Hodgman, M. Schreiber, S. Sarkar, A. J. Daley, M. H. Fischer, E. Altman, I. Bloch, U. Schneider, *Phys. Rev. X* **7**, 011034 (2017).
- [5] T. Tomita, S. Nakajima, I. Danshita, Y. Takasu, and Y. Takahashi, arxiv:1705.09942 (2017).
- [6] S. Diehl, A. Micheli, A. Kantian, B. Kraus, H. P. Bchler, and P. Zoller, *Nature Physics* **4**, 878 (2008).
- [7] P. Schindler, M. Müller, D. Nigg, J.T. Barreiro, E.A. Martinez, M. Hennrich, T. Monz, S. Diehl, P. Zoller, and R. Blatt, *Nature Phys.* **9**, 361 (2013).
- [8] T. Giamarchi, and H. J. Schulz, *Europhys. Lett.* **3**, 1287 (1987).
- [9] M. P. A. Fisher, P. B. Weichman, G. Grinstein, and D. S. Fisher, *Phys. Rev. B* **40**, 546 (1989).
- [10] D. Jaksch, C. Bruder, J. I. Cirac, C. W. Gardiner, and P. Zoller, *Phys. Rev. Lett.* **81**, 3108 (1998).
- [11] G. Lindblad, *Commun. Math. Phys.* **48**, 119 (1976).
- [12] V. Gorini, k. Kossakowski, and E. Sudarshan, *J. Math. Phys.* **17**, 821 (1976).
- [13] H. Breuer and F. Petruccione, *The theory of Quantum Open Systems* (Oxford Univ. Press, Oxford, 2002).
- [14] C. W. Gardiner and P. Zoller, *Quantum Noise* (2000).
- [15] U. Weiss, *Quantum Dissipative Systems* (Series in Modern Condensed Matter Systems, Singapore, 2008).
- [16] V. S. E. Mascarenhas, G. Giudice, arxiv:1703.02934 (2017).
- [17] V. S. J. Reisons, E. Mascarenhas, arxiv:1706.08272 (2017).
- [18] A. V. Ponomarev, S. Denisov, and P. Hänggi, *Phys. Rev. Lett.* **106**, 010405 (2011).
- [19] A. De Luca, J. Viti, L. Mazza, and D. Rossini, *Phys. Rev. B* **90**, 161101(R) (2014).
- [20] A. Biella, A. De Luca, J. Viti, D. Rossini, L. Mazza, and R. Fazio, *Phys. Rev. B* **93**, 205121 (2016).
- [21] T. P. M. Ljubotina, M. Znidaric, arxiv:1702.04210 (2017).
- [22] Z. Cai, U. Schollwöck, and L. Pollet, *Phys. Rev. Lett.* **113**, 260403 (2014).
- [23] Z. Cai, Z. Yan, L. Pollet, J. Lou, X. Wang, and Y. Chen, arxiv:1704.00606 (2017).
- [24] U. Schollwöck, *Annals of Physics* **326**, 96 (2011).
- [25] F. Verstraete, J. J. García-Ripoll, and J. I. Cirac, *Phys. Rev. Lett.* **93**, 207204 (2004).
- [26] M. Zwolak and G. Vidal, *Phys. Rev. Lett.* **93**, 207205 (2004).
- [27] A. J. Daley, *Adv. Phys.* **63**, 77 (2014).
- [28] I. de Vega and M.-C. Bañuls, *Phys. Rev. A* **92**, 052116 (2015).
- [29] K. G. Wilson, *Rev. Mod. Phys.* **47**, 773 (1975).
- [30] J. Prior, A. W. Chin, S. F. Huelga, and M. B. Plenio, *Phys. Rev. Lett.* **105**, 050404 (2010).
- [31] A. W. Chin, A. Rivas, S. F. Huelga, and M. B. Plenio, *J. Math. Phys.* **51**, 092109 (2010).
- [32] T. D. Kühner, S. R. White, and H. Monien, *Phys. Rev. B* **61**, 12474 (2000).
- [33] I. de Vega and D. Alonso, *Rev. Mod. Phys.* **89**, 015001 (2017).
- [34] I. de Vega, U. Schollwöck, and F. A. Wolf, *Phys. Rev. B* **92**, 155126 (2015).
- [35] See supplementary material.
- [36] In this case, since the total quantum number of the system plus environment is conserved, we use a number conserving MPS time evolution algorithm.
- [37] E. M. Stoudenmire and S. R. White, *New J. Phys.* **12**, 055026 (2010).
- [38] Due to the finite coupling between the system and the bath, especially for small ΔE , the system evolution will not be completely frozen, however, no decay, even over long times, is expected.
- [39] The time interval in which the slope is computed is chosen so that the signal is not strongly affected by the initial oscillations, and that the slope is fairly constant (except close to the transition).

- [40] We evaluate the groundstate energy using density matrix renormalization group (DMRG) [24] for $N = L$ and $N = L - 1$ for system sizes up to 120, keeping 5000 states and a local cut-off up to 5 bosons per site. This gives an accuracy of 4 significant digits on the total energy.
- [41] For $L = 10$, ΔE crosses 0 for $U \approx 2.84$.
- [42] D. Dalidovich and M.P. Kenneth, Phys. Rev. A., **79** 053611, (2009).
- [43] It is interesting to point out that the stable-unstable transition is consistent with Fermi golden rule, when considering all the decaying channels of the system as described in [50], although the latter cannot correctly predict the short time dynamics.
- [44] D. S. Rokhsar and B. G. Kotliar, Phys. Rev. B **44**, 10328 (1991).
- [45] W. Krauth, M. Caffarel, J.P. Bouchaud, Phys. Rev. B **45**, 3137 (1992).
- [46] Within the Gutzwiller approach, the wavefunction of the system plus bath is described by $|\psi\rangle = \otimes_l (\sum_n f_{n,l}|n\rangle_l)$ where l spans all the sites of the system and the bath, while $|n\rangle_l$ means n bosons at site l . In the Mott-insulating regime, at unit filling the $f_{n,j}$ in the system are given by $f_{n,j} = \delta_{n,1}$ where $\delta_{n,m}$ is the Kronecker δ , while for a $T = 0$ bath $f_{n,j} = \delta_{n,0}$. It follows that $\langle \hat{\alpha}_j \rangle = 0$ and $\langle \hat{c}_j \rangle = 0$ and hence the dynamics steered by the tunnelling term in the Hamiltonian is completely frozen.
- [47] I. de Vega, D. Porras, and J. Ignacio Cirac, Phys. Rev. Lett. **101**, 260404 (2008).
- [48] P. Zupancic, P.M. Preiss, R. Ma, A. Lukin, M.E. Tai, M. Rispoli, R. Islam, and M. Greiner, Opt. Exp. **24**, 13881 (2016).
- [49] A. Recati, P.O Fedichev, W. Zwerger, J. von Delft, and P. Zoller, Phys. Rev. Lett **94**, 040404 (2005).
- [50] G. Schaller, *Open Quantum Systems Far from Equilibrium; Lecture Notes in Physics*, Springer: Berlin/Heidelberg, Germany (2014).

Appendix A: Chain representation

Instead of simulating the dynamics due to the discretized version of Eq.(1-3), we map the bath to a long linear chain with only nearest neighbor coupling with what is known as the ‘‘star-to-chain’’ mapping [29–31, 34].

The Hamiltonian then becomes

$$\begin{aligned} \hat{H}_{\text{tot}}^{\text{dis},'} &= \hat{H}_S + \sum_{j=1}^{N'_{\text{max}}} \Omega_j \hat{c}_j^\dagger \hat{c}_j + \beta_0 (\hat{\alpha}_L^\dagger \hat{c}_1 + \hat{\alpha}_L \hat{c}_1^\dagger) \quad (\text{A1}) \\ &+ \sum_{j=1}^{N'_{\text{max}}-1} \beta_j (\hat{c}_j^\dagger \hat{c}_{j+1} + \hat{c}_{j+1}^\dagger \hat{c}_j), \end{aligned}$$

where $\beta_0 = J\sqrt{\sum_{j=1}^{N'_{\text{max}}} \mathcal{J}_j}$. In order to ensure that $\hat{H}_{\text{tot}}^{\text{dis},'}$ dictates the same dynamics as $\hat{H}_{\text{tot}}^{\text{dis}}$, we used different $N'_{\text{max}} < N_{\text{max}}$ until the observables converged (we have used $N'_{\text{max}} = 200$ except for the case of $N = L = 2$ for which we have used $N'_{\text{max}} = 400$). To evaluate the other coefficients α_j and β_j we have performed a Lanczos tridiagonalization which, via a unitary matrix U converts a

diagonal matrix $\mathbf{M} = \text{diag}(\omega_1, \omega_2, \dots, \omega_{N_{\text{max}}})$ to a tridiagonal matrix \mathbf{T} via $\mathbf{M}_E \mathbf{U} \approx \mathbf{U} \mathbf{T}$. The coefficients of \mathbf{T} are the Ω_j and β_j :

$$\mathbf{T} = \begin{pmatrix} \Omega_1 & \beta_1 & 0 & \dots \\ \beta_1 & \Omega_2 & \beta_2 & \dots \\ \vdots & \vdots & \vdots & \vdots \\ 0 & 0 & \beta_{N'_{\text{max}}-1} & \Omega_{N'_{\text{max}}} \end{pmatrix}. \quad (\text{A2})$$

For more details see [34]. Since the transformation is unitary, the operators \hat{c}_j obey the same bosonic commutation relations as the \hat{b}_j .

Appendix B: Thermofield transformation

With the thermofield transformation [28], the environment oscillators \hat{b}_j are mapped to $2N_{\text{max}}$ oscillators $\hat{a}_{1,j}$ and $\hat{a}_{2,j}$, with the new Hamiltonian $\hat{H}_{\text{tot}}^{\text{tf}}$

$$\begin{aligned} \hat{H}_{\text{tot}}^{\text{tf}} &= \hat{H}_S + \sum_{j=1}^{N_{\text{max}}} \omega_j (\hat{a}_{1,j}^\dagger \hat{a}_{1,j} - \hat{a}_{2,j}^\dagger \hat{a}_{2,j}) \quad (\text{B1}) \\ &+ \sum_{j=1}^{N_{\text{max}}} g_{1,j} (\hat{\alpha}_L^\dagger \hat{a}_{1,j} + \hat{\alpha}_L \hat{a}_{1,j}^\dagger) \\ &+ \sum_{j=1}^{N_{\text{max}}} g_{2,j} (\hat{\alpha}_L \hat{a}_{2,j} + \hat{\alpha}_L^\dagger \hat{a}_{2,j}^\dagger), \end{aligned}$$

where $g_{1,j} = J\sqrt{\mathcal{J}_j} \cosh(\theta_j)$ and $g_{2,j} = J\sqrt{\mathcal{J}_j} \sinh(\theta_j)$, with $\cosh(\theta_j) = \sqrt{1+n(\omega_j)}$, $\sinh(\theta_j) = \sqrt{n(\omega_j)}$ and $n(\omega) = 1/(e^{\omega/T} - 1)$. After star-to-chain mapping the Hamiltonian we study is

$$\begin{aligned} \hat{H}_{\text{tot}}^{\text{tf},'} &= \hat{H}_S + \sum_{j=1}^{N'_{\text{max}}} \Omega_{1,j} \hat{a}_{1,j}^\dagger \hat{a}_{1,j} + \beta_{1,0} (\hat{\alpha}_L^\dagger \hat{a}_{1,1} + \hat{\alpha}_L \hat{a}_{1,1}^\dagger) \\ &+ \sum_{j=1}^{N'_{\text{max}}-1} \beta_{1,j} (\hat{a}_{1,j}^\dagger \hat{a}_{1,j+1} + \hat{a}_{1,j+1}^\dagger \hat{a}_{1,j}) \\ &+ \sum_{j=1}^{N'_{\text{max}}} \Omega_{2,j} \hat{a}_{2,j}^\dagger \hat{a}_{2,j} + \beta_{2,0} (\hat{\alpha}_L \hat{a}_{2,1} + \hat{\alpha}_L^\dagger \hat{a}_{2,1}^\dagger) \\ &+ \sum_{j=1}^{N'_{\text{max}}-1} \beta_{2,j} (\hat{a}_{2,j}^\dagger \hat{a}_{2,j+1} + \hat{a}_{2,j+1}^\dagger \hat{a}_{2,j}). \quad (\text{B2}) \end{aligned}$$

Appendix C: Redfield master equation

We use the following master equation

$$\begin{aligned} \frac{d\hat{\rho}_S(t)}{dt} = & -i[H_S, \hat{\rho}_S] + \int_0^t d\tau \chi^+(\tau) [V_{-\tau}(\hat{\alpha}_L^\dagger) \hat{\rho}_S(t), \hat{\alpha}_L] \\ & + \int_0^t d\tau \chi^-(\tau) [V_{-\tau}(\hat{\alpha}_L) \hat{\rho}_S(t), \hat{\alpha}_L^\dagger] + \text{H.c.}, \end{aligned} \quad (\text{C1})$$

where $\chi^-(t) = \sum_j \mathcal{J}_j [n(\omega_j) + 1] e^{-i\omega_j t}$, $\chi^+(t) = \sum_j \mathcal{J}_j n(\omega_j) e^{i\omega_j t}$ and the ω_j are the system eigenvalues. We have also used $V_\tau(X) = \hat{U}_S^{-1}(\tau, 0) X \hat{U}_S(\tau, 0)$, where $\hat{U}_S(\tau, 0) = e^{-i\hat{H}_S \tau}$ [33].

Appendix D: Two sites and two bosons case

In this case only a few energy levels are relevant for the dynamics. As initial condition we take the ground-state for $N = L = 2$, whose energy is $E_{N=2}^0 = (U - \sqrt{16 + U^2})/2$. For $L = 2$ and $N = 1$ there are only two eigenstates $|E_{N=1}^{0,1}\rangle$ with energies, $E_{N=1}^{0,1} = \mp 1$, hence only $|E_{N=1}^0\rangle$ can have energy lower than $E_{N=2}^0$, but only for $U > 3$ (because of finite size effects the critical value is 3 and not ≈ 2.82). The dynamics between these two states is described by the effective Hamiltonian

$$\begin{aligned} \hat{H} = & \sum_{\omega} \gamma \sqrt{\mathcal{J}(\omega)} (|E_{N=2}^0\rangle \langle 0|_b \langle E_{N=1}^0| \langle \omega|_b + \text{H.c.}) \quad (\text{D1}) \\ & + E_{N=2}^0 |E_{N=2}^0\rangle \langle E_{N=2}^0| + E_{N=1}^0 |E_{N=1}^0\rangle \langle E_{N=1}^0| \\ & + \sum_{\omega} \omega |\omega\rangle_b \langle \omega|_b. \end{aligned}$$

Here $|\omega\rangle_b$ is a state with a single oscillator mode ω occupied, while γ is the coupling between the two states $|E_{N=2}^0\rangle$ and $|E_{N=1}^0\rangle$ due to $\hat{\alpha}_2^\dagger$ acting on the second site. This can be computed by transforming $\hat{\alpha}_2^\dagger$ into the eigenbasis of these two number sectors giving $\gamma = (4 - U + \sqrt{16 + U^2}) / (2\sqrt{16 + U^2} - U\sqrt{16 + U^2})$. Eq.(D1) describes a two-level system coupled with vacuum, which can be solved analytically [33].

Appendix E: Bath coupled to each site

The stable-unstable transition is due to the presence, or absence, of a global energy gap of the system+bath set-up. If the energy of the ground state for $N = L$ bosons is lower than the energy of the ground state for $N = L - 1$ bosons, and if the system is coupled to a $T = 0$ bath, then the system is stable and will not lose bosons, independently of whether one or more sites are coupled to the bath. To demonstrate this we consider again a small system with $N = L = 2$ for the cases in

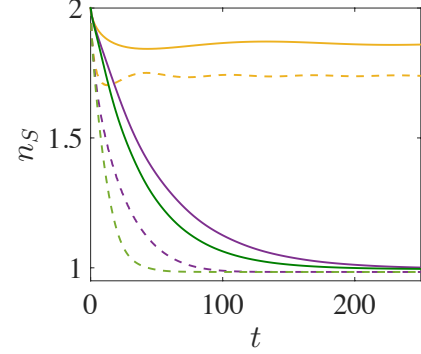


FIG. 5: (color online) Total number of bosons in the system as a function of time t . The continuous lines correspond to the case of one site coupled to the bath, while the dashed lines to two sites. The curves correspond, from top to bottom, to $U = 3, 4$ and 5 . The other common parameters are $g = 0.01$, $\eta = 0.5$ and $T = 0$. Here we have chosen $N = L = 2$.

which one or two sites are coupled to the bath. In Fig.5 we show that qualitatively the time-dependence of the number of particles is independent of whether only one or two sites are coupled to the bath. The main difference is only quantitative, in fact, as expected, we observe that the decay is faster when both sites are coupled to the bath.